Experimental investigation of a control scheme for a zero-detuning resonant sideband extraction interferometer for next-generation gravitational-wave detectors

Fumiko Kawazoe* and Akio Sugamoto
Ochanomizu University, 2-1-1 Otsuka,
Bunkyo-ku, Tokyo 112-8610, Japan

Volker Leonhardt, Shuichi Sato, Toshitaka Yamazaki, Mitsuhiro Fukushima, Seiji Kawamura
National Astronomical Observatory of Japan, 2-21-1 Osawa, Mitaka-shi, Tokyo 112-8610, Japan

Osamu Miyakawa
LIGO Laboratory, California Institute of Technology, Pasadena, CA 91125, USA

Kentaro Somiya
Max-Planck-Institut für Gravitationsphysik, Am Mühlenberg 1, 14476 Potsdam, Germany

Tomoko Morioka
University of Tokyo, Kashiwa, Chiba 277-8582, Japan

Atsushi Nishizawa
Kyoto University, Yoshida-Honmachi, Sakyo-ku, Kyoto 606-8501, Japan
(Dated: March 19, 2008)

Some of next-generation gravitational-wave detectors, such as the American Advanced LIGO project and the Japanese LCGT project, plan to use power recycled resonant sideband extraction (RSE) interferometer as the optical configuration for their interferometers. A power recycled zero-detuning (PRZD) RSE interferometer, which is the default design for LCGT, has five degrees of freedom that need to be controlled in order to operate a gravitational-wave detector, although it is expected to be very challenging because of the complexity of its optical configuration. A new control scheme for a PRZD RSE interferometer has been developed and tested with a prototype interferometer. The PRZD RSE interferometer was successfully locked with the control scheme. It is the first experimental demonstration of a PRZD RSE interferometer with suspended test masses. The result serves as an important step for the operation of LCGT.

I. INTRODUCTION

Presently several laser interferometer gravitational-wave detectors are in operation in the United States, (LIGO[1]), in Europe, (GEO600[2], and VIRGO[3]), and in Japan, (TAMA300[4]). In addition to the present detectors, there are plans to upgrade them to next-generation interferometers. Amongst them are Advanced LIGO[5] and LCGT[6], which plan to use the power recycled resonant sideband extraction (RSE) technique to enhance detector sensitivities. The LCGT plans to use a power recycled zero-detuning (PRZD) RSE configuration while Advanced LIGO plans to use a power recycled detuned RSE configuration.

Despite the great advantage that it is able to achieve better sensitivity by avoiding problems of thermal absorption by substrates, the RSE configuration poses a more difficult challenge in controlling the interferometer in order to use it as a gravitational-wave detector due to the increased number of degrees of freedom (DOF) that need to be controlled. Therefore, designing a control scheme as simple as possible, and demonstrating it are vital before the technique is adapted in large-scale interferometers such as LCGT.

We have developed a control scheme for LCGT[7], and have carried out experimental work[8]. This experiment aims to control a PRZD RSE interferometer using the scheme, and to measure the sensing matrix and compare it with modeling. The control scheme is described in section II, the experimental results are presented in section III, the results are shown in section IV, discussions are presented in section V, and finally the conclusion is presented in section VI.

II. CONTROL SCHEME

The control scheme consists mainly of two parts; the signal extraction scheme and the lock sequence.

---

*Electronic address: kawazoe@gravity.mtk.nao.ac.jp

A. Signal extraction scheme

The power recycled RSE interferometer has five DOFs to be controlled as shown in Fig. 1. They are the average length and the differential length of the two Fabry-Perot (FP) arm cavities, L_+, and L_-, respectively, as indicated by arrows with solid lines, the average length and the differential length of the power recycling cavity (PRC), l_+, and l_-, respectively, as indicated by arrows with short dashed lines, and the average length of the signal extraction cavity (SEC), l_s, as indicated by arrows with long dashed lines.
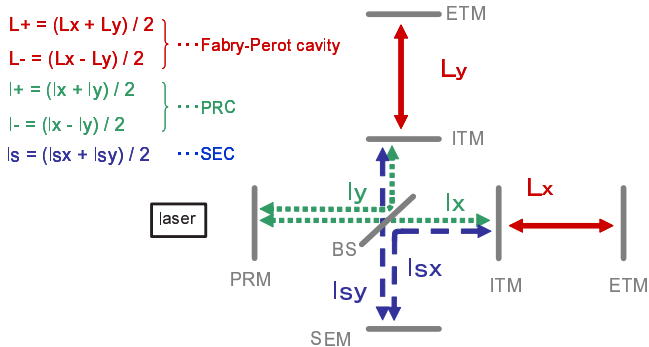

FIG. 1: Degrees of freedom in the power recycled RSE interferometer.

It is known from experience with present detectors which use the Pound-Drever-Hall (PDH) method that the arm cavities are relatively easy to control with clean control signals as the arm cavities have high finesse. On the other hand, it is expected to be quite challenging to obtain clean control signals of the central part of the RSE, because the resonant conditions of the light fields inside the central part will be strongly affected by both the PRC and the SEC. Thus the length sensing scheme has to be designed in such a way that it manipulates the resonant conditions of the light inside by properly designing cavity lengths and sideband frequencies.

The outline of the length sensing scheme is as follows. It is based on the PDH method. The FP arm cavity lengths are controlled with a single modulation-demodulation technique and the central part of the RSE is controlled with a double modulation-demodulation technique with amplitude modulation (AM) sidebands and phase modulation (PM) sidebands. By using the double modulation-demodulation technique, the control signals for the central part will be affected very little by the signals derived from the carrier which are dominated by the FP arm cavities. This is because both the AM and the PM modulation sideband frequencies are designed in such a way that they are not resonant in the FP arm cavities; thus it decouples the FP arm cavities and the central part.

1. The central part

The central part is designed so that the AM and the PM sidebands behave in the following way. The lengths of two paths that compose the Michelson interferometer have a macroscopic asymmetry such that when the carrier interferes destructively at the dark port (DP), the AM sidebands interfere constructively at the bright port (BP) and destructively at the DP, while the PM sidebands interfere destructively at the BP and constructively at the DP. Thus the AM sidebands "reflect completely" from the Michelson part while the PM sidebands "transmit completely" through the Michelson part. This condition is met when the round trip Michelson asymmetry length is designed to be equal to $(2m + 1)/2$ $(m = 0, 1, 2, ...)$ times the wavelength λ for the AM sidebands and integer multiple of the wavelength for the PM sidebands. In our design it is 3λ for the AM sidebands and $\frac{1}{2}\lambda$ for the PM sidebands. Two cavities' macroscopic lengths are designed so that the AM sidebands resonate inside the PRC and the PM sidebands resonate inside the compound cavity made of the PRC and the SEC. This enables the PM sidebands to be sensitive to the length of the SEC while the AM sidebands is not affected by the SEC length, thus ensuring independent control signals for l_+ and l_s.

2. The whole RSE

Figure 2 shows how the control signals of the prototype RSE interferometer are obtained. The L_+ control signal is obtained at BP and is fed-back to the end test masses (ETM), the L_- control signal is obtained at DP and is fed-back to the ETMs. The l_- control signal is obtained at DP and is fed-back to the beam splitter (BS), the l_+ control signal is obtained at the BP and is fed-back to the power recycling mirror (PRM), and the l_s control signal is obtained at the pick-off port (PO) and is fed-back to the signal extraction mirror (SEM).

Table I shows the theoretical length sensing signal matrix. The signals are at DC. It is calculated with parameters used for the prototype RSE interferometer, of which there will be a detailed explanation in section III. Demodulation phases are chosen so that each main signal (i.e. the signal that should be obtained at the corresponding detection port) is maximized. The first from the left column shows the detection ports; SD and DD stand for single/double modulation-demodulation, respectively, and the top first raw shows the DOFs. The values are normalized by each main signal. The L_+ and L_- signals are dominant at BP and DP, respectively due to the designed high finesse of the Fabry-Perot arms, indicating they are relatively easy to obtain. On the other hand, it is obvious from the matrix that l_+ and l_s signals mix each other at both BP and PO. However, the degree to which they mix each other is such that linearly independent signals can be obtained. Also $L_{+/-}$ signals that mix with the

main signals on the DD systems are relatively small due to the fact that the carrier is not used for them. [12] This is necessary to bring the interferometer from an uncontrolled state to a controlled state. Therefore the designed control scheme is a promising approach for acquiring the control.
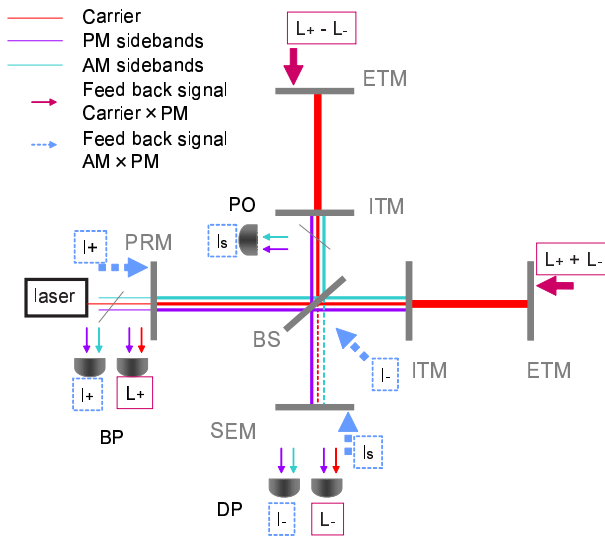

FIG. 2: Control of the whole interferometer.

TABLE I: Theoretical matrix

	L_+	L_-	l_+	l_-	l_s
BP(SD)	1	8.2×10^{-6}	-2.6×10^{-2}	6.4×10^{-4}	1.3×10^{-2}
DP(SD)	-9.2×10^{-9}	1	5.9×10^{-9}	1.3×10^{-2}	8.6×10^{-9}
BP(DD)	-4.9×10^{-2}	-1.1×10^{-4}	1	-8.6×10^{-3}	-5.3×10^{-1}
DP(DD)	-1.0×10^{-4}	7.6×10^{-2}	1.4×10^{-3}	1	1.1×10^{-5}
PO(DD)	-1.5×10^{-1}	-1.2×10^{-2}	1.1	-2.2×10^{-2}	1

B. Lock sequence

Up until this point we had assumed that the interferometer is close to its operating point; therefore feedback signals for all the DOFs are always present for the control system to work properly. In reality the uncontrolled interferometer is not near its operating point most of the time, therefore feedback signals for all the DOFs are not present simultaneously. In order to successfully lock the interferometer a sequence of the lock needs to be established. Here we show one possible order to lock the whole interferometer with simulation work results. The sequence is as follows.

1. Lock the central part

    (a) Lock l_- DOF

    (b) Lock l_+ DOF

    (c) Lock l_s DOF

2. Lock the FP arm cavities

Figure 3 shows the feedback signal of the l_- DOF when the other two DOFs of the central part are free of control. Here the FP arms are assumed not to be present for simplicity. The plots are contour plots of the error signal for the l_- DOF when the other two DOFs are uncontrolled, i.e. the microscopic position of the PRM expressed in the phase gained by the light (hereinafter called phi) is scanned from its operating point by 0, 30, 60, and 90 degrees as indicated by the vertical arrow, while the SEM's phi is scanned from its operating point by -90 to 90 degrees in the direction of the y-axis. The x-axis shows the phi of the l_- DOF, with the phi = 0 being the operating point. On the right of each plot there is a color bar that shows the signal amplitude.

The l_- DOF can be locked to where the amplitude of the error signal changes its sign, so called the zero crossing. A clear vertical line of a zero crossing is present at the operating point in the top figure when the l_+ and the l_s DOFs happen to be at their operating points, (i.e. their phi are zero). The polarity of the zero crossing needs to be taken into account; in this case the right polarity is the one that goes from plus to minus as the phi is moved from minus to plus. With the wrong polarity even if there is a zero crossing at the operating point, different light field could be resonant in the cavity of interest, so the DOF is no longer locked to the original operating point. A zero crossing line at the operating point having the wrong polarity is seen as the phi of the l_s DOF is scanned between 0 to 90 degrees. One such example is marked by the ellipse in the figure. According to the simulation results the chance of such a line being present is $\sim 30\%$ at the maximum. This indicates that most of the time (with minimum chance of being $\sim 70\%$) when the other two DOFs are completely free of control, (i.e. their detunings are scanned independently from each other), the l_- DOF can be locked to its operating point.

Then, with the assumption that the l_- is now locked to its operating point, the feedback signal of the l_p DOF is shown in Fig. 4 when the l_s is still free of control so it could be anywhere in the y-axis. In the same manner as in Fig. 3, it is clear that a zero crossing for the l_p is present at very close to its operating point regardless of the l_s's phi detuning. Therefore the l_+ DOF can be locked to its operating point. When this is the case the zero crossing line of the l_- DOF is always present as shown in the top plot of Fig. 3 so the lock of the l_- DOF becomes stable.

Then next as well as with the same assumption that the l_- is locked, with a new assumption that the l_+ is locked to its operating point, a feedback signal of the l_s DOF is shown in Fig. 5. From the figure it is shown that a zero crossing point is present at its operation point as marked by the arrow. In this way the central part is locked to its operating point.

This is a good approximation because the chance that the carrier is resonant inside the FP arm cavities and thus disturbs the central part length sensing signals is very

small because of the high finesse, and the chance that the sidebands are accidentally resonant inside the FP arm cavities are very small because of the same reason.

Next the FP arms are locked by acquiring the lock of the individual FP arm whose control signal is always present and dominant at each detection port for each FP arm cavity. Once the two FP arm cavities are locked the control servos can be switched to those of the L_- and L_+ DOF to change them into the controls of L_- and L_+ DOFs simultaneously. Therefore the FP arms are locked. Thus the whole RSE interferometer can be locked in this order.

III.   EXPERIMENTAL DEMONSTRATION OF A CONTROL OF THE PRZD RSE

A.   4m Prototype interferometer

Figure 6 shows the optical layout of the prototype interferometer. A light at 1.064 μm from a Nd:YAG laser enters a Mach-Zehnder interferometer (MZ) where two Pockels cells are placed in different paths of the MZ and it is phase modulated at 17.25 MHz and amplitude modulated at 103.25 MHz. Light power at the output of the MZ is 90 mW with modulation depths of approximately 0.15 rad. The FP arm cavity length is 4.15m and is formed by a flat input mirror and a curved end mirror with a radius of curvature of 6m. Two mode-matching lenses are used for the FP arm cavities and additional two are used to compensate for the mismatch due to the relatively large Michelson macroscopic length asymmetry (4.35 m). The coupling ratio between the incident beam and the fundamental mode of the FP arm cavity of more than 98% is realized. The finesse of the cavity is approximately 120. All of the seven test masses (diameter 2.54cm) are suspended as double pendulums (height 30cm) to suppress the mirror motion at frequencies above the resonant frequency (at about 1.5Hz). The test mass motion around its resonant frequency is damped by an eddy current damping system. The length control is performed via coil-magnets actuators.

B.   Lock Sequence

The lock of the RSE has been successfully demonstrated. The sequence that has been determined with the simulation work is used; the central part first then the FP arm cavities next.[13]

We define several lock states, which are shown in Fig. 7. Each state is indicated as follows.

- State 0 : The interferometer is uncontrolled.

- State 1 : Michelson is locked to dark fringe at the DP.
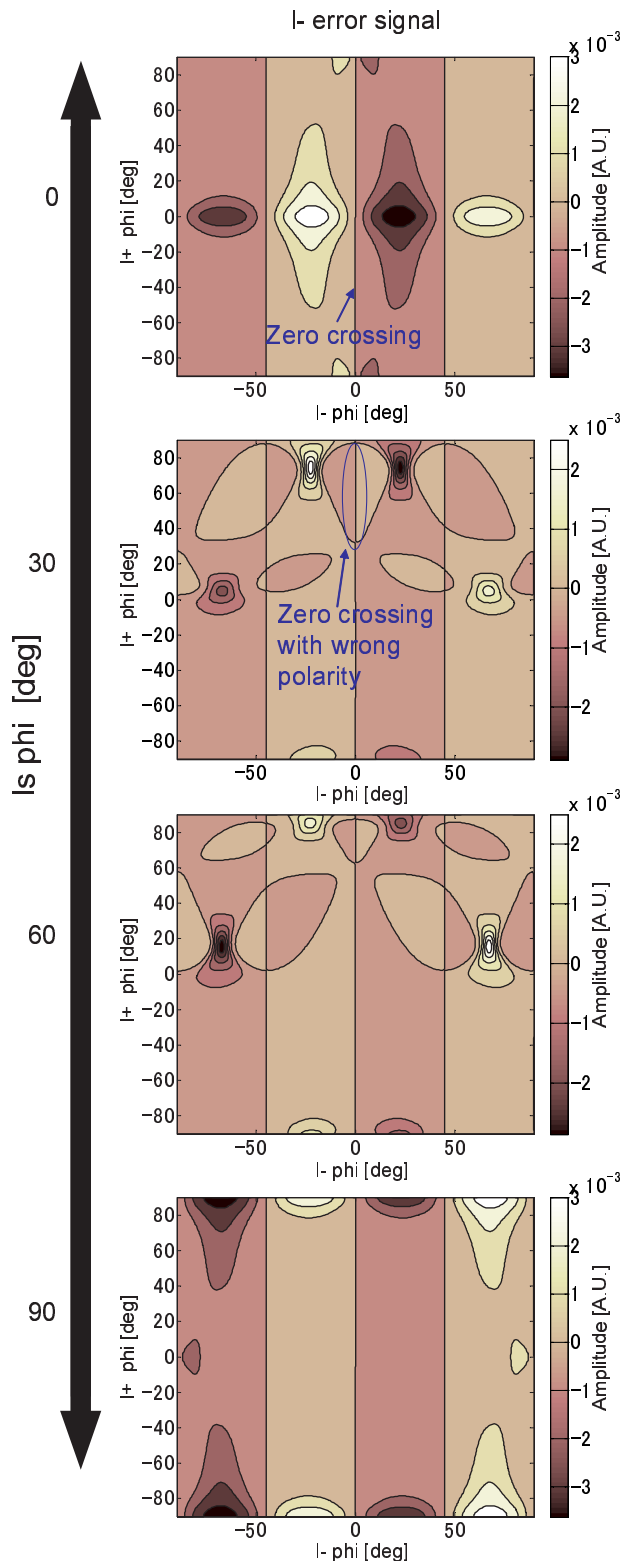
- State 2 : Power-recycled Michelson is locked.

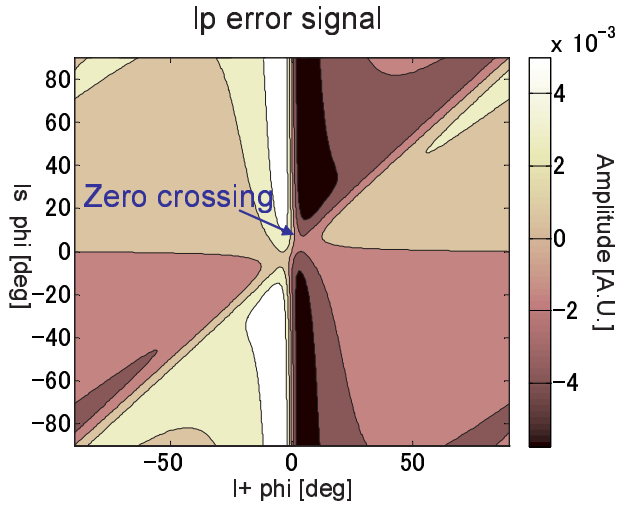FIG. 3: l_- error signal with SEM and PRM free.

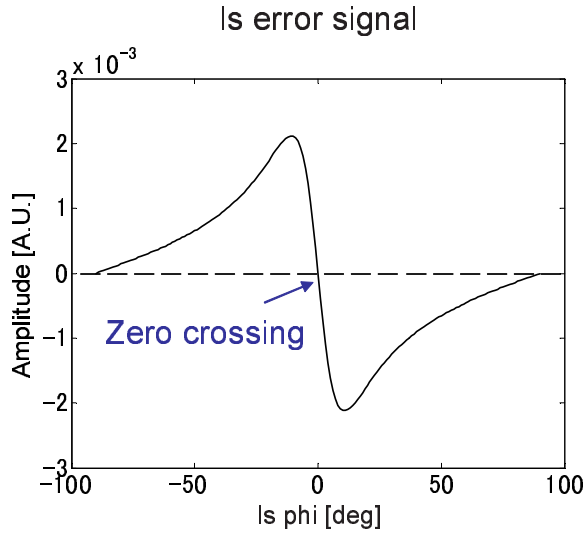FIG. 4: l_+ error signal with SEM free and l_- in lock.

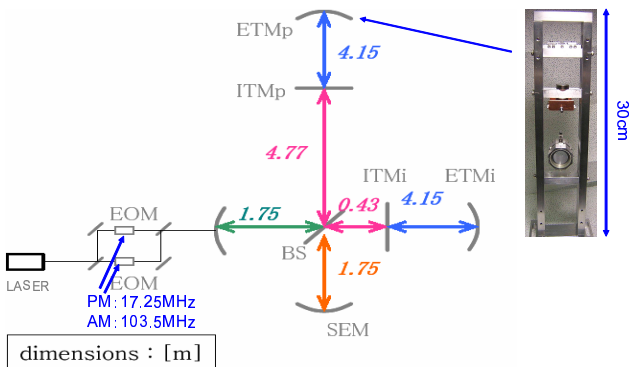FIG. 5: l_s error signal with l_+ and l_- in lock.

FIG. 6: Optical layout of the prototype interferometer.

- State 3 : Central part is locked.

- State 4 : Tuned RSE is locked

In state 2, the carrier is anti-resonant inside the PRC. In order for the carrier to be resonant inside the PRC, the phase needs to be shifted by π inside the PRC, which happens when the carrier is resonant inside the FP arm cavities as in state 4. Figure 8 shows the DC power detected at various ports, (i.e. DP, BP, PO, transmitted port for the inline FP arm cavity and for the perpendicular FP arm cavity). Each lock state is separated with boxes with colors specified in Fig. 7, and on top of each box the state number is shown. The start time of each state is defined as the time when the switch of a servo loop of each DOF is turned on. Typically each DOF is locked within a fraction of a second after the servo loop is switched on. Between the time 10 and 20 sec, the l_- DOF is not locked the whole time. This is because the carrier is not yet anti-resonant inside the PRC and disturbers the control signal of the l_- DOF. When the l_+ servo loop is switched on at time 20 sec, the carrier is anti-resonant inside the PRC and the l_- DOF is completely locked as well as the l_+ DOF. The difference between the state 2 and 3 is not obvious from the DC signals, due to the relatively small size of the modulation sidebands compared to that of the carrier. The sharp peaks seen between time 20 and 40 sec can be explained as follows. The carrier light is sometimes resonant in one of the two arms, consequently adding a relative phase shift of π between the two beams interfering at the BS. This will switch the DP into BP, and vice versa, so the DP is no longer dark. Note that the corresponding peaks in transmitted light from the FP arm cavities are too small to be seen in the plots.

In order to verify the locking status, resonant conditions for the two sets of sidebands are monitored with optical spectrum analyzers (OSA) placed at the DP and the PO. Figure 9 shows the output of the optical spectrum analyzers. The upper three plots show the output power at the PO and the bottom three show the output power at the DP. Colored boxes indicate the lock state, as specified in Fig. 7. In state 1, neither the AM nor the PM sidebands are resonant. In state 2, the AM sidebands are resonant inside the PRC, thus there are resonant peaks of the AM sidebands detected at the PO. The PM sidebands are not yet resonant. In state 3, the PM sidebands are resonant inside the compound cavity made of the PRC and the SEC thus there are resonant peaks of the PM sidebands detected at the DP. Each cavity length is controlled throughout the locking process.

Table II shows the measured length sensing signal matrix, normalized by the main signals at each detection port. Demodulation phases are tuned to maximize the main signal at each detection ports. A sinusoidal signal is applied to a feedback path of each DOF to move the test masses. The signal frequency (at 2.2 kHz) is well above the unity gain frequency of all the control servo so that loop gains do not have to be taken into account.
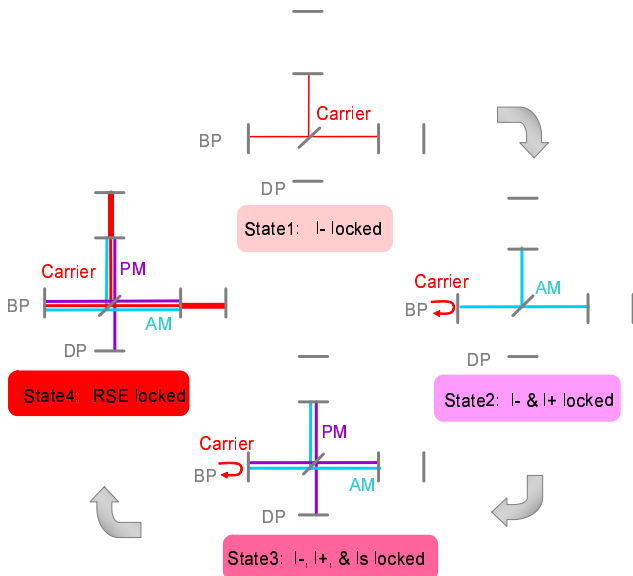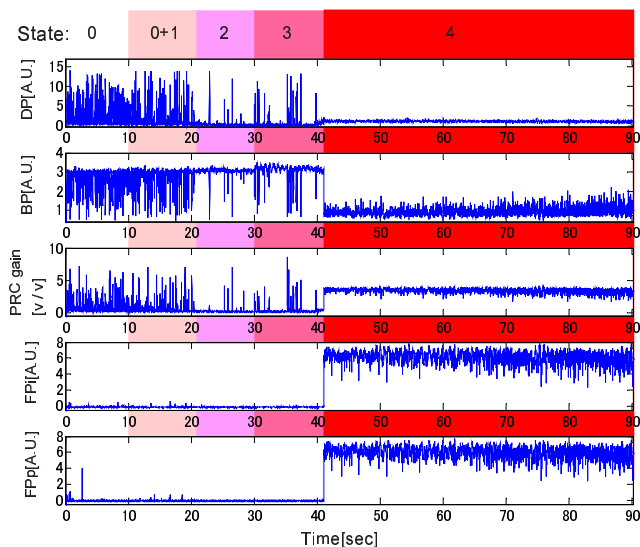
FIG. 7: Lock states of the interferometer.

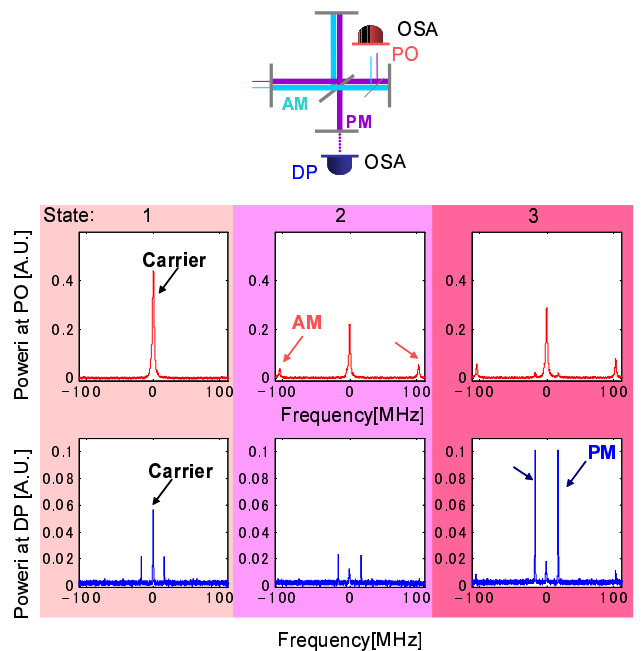FIG. 8: DC power at various ports.

FIG. 9: Sideband resonant peaks inside the PRC and the SEC.

where agreement in the overall feature of the matrix is of importance in order to verify the control scheme.

TABLE II: Measured normalized matrix

	L_+	L_-	l_+	l_-	l_s
BP(SD)	1	4.5×10^{-2}	4.8×10^{-2}	-1.9×10^{-2}	-1.3×10^{-2}
DP(SD)	-1.9×10^{-1}	1	-2.1×10^{-3}	-4.9×10^{-2}	-1.5×10^{-3}
BP(DD)	-1.2×10^{-1}	6.6×10^{-3}	1	1.8×10^{-2}	-5.0×10^{-2}
DP(DD)	-1.1×10^{-1}	-3.1×10^{-1}	1.1×10^{-1}	1	1.2×10^{-1}
PO(DD)	-1.1	2.2×10^{-1}	4.0×10^{-1}	5.1×10^{-1}	1

IV. RESULTS

The lock of the PRZD RSE has been successfully demonstrated with the prototype interferometer. It is the first experimental demonstration of a PRZD RSE interferometer with suspended test masses. In parallel the control sequence has been established with a simulation work. The measured signal matrix showed good agreement with modeling.

V. DETERIORATION OF QUANTUM NOISE LIMITED SENSITIVITY VIA FEEDBACK LOOPS

The results of this experiment clearly shows that the newly developed control scheme can be used to bring the interferometer from an uncontrolled state to a con-

The frequency is also well below the cut-off frequency of the optical response of the RSE (at about 1 MHz), so the values can be directly compared with the theoretical DC values.

The general pattern of the measured matrix is in good agreement with the theoretical one; the $L_{+/-}$ signals dominate at their detection ports, the l_+ and the l_s mix at BP and PO but the signals are linearly independent, and the $L_{+/-}$ signals that mix at DD systems are relatively small. In general other unwanted signals than the one that should be obtained at the corresponding detection ports tend to be greater than the theoretical values due to present imperfections such as the unwanted carrier light at the DP. It is not essential for this experiment

trolled state. Once the interferometer is controlled it needs to perform at its best sensitivity. The sensitivity of the next-generation interferometers are expected to be limited by the fundamental quantum noise in the laser, namely the radiation pressure noise and the shot noise at their observation bands[9].

Only the shot noise level is subject to a control scheme. The quantum noise limited sensitivity could be deteriorated via feed-back signals that are necessary for the control system, i.e, when the shot noise on the control signal of L_- DOF is increased by the shot noise on feed-back signals of the other DOFs via the off-diagonal elements of the signal matrix and if they add great enough noise, the overall sensitivity is deteriorated. In order to evaluate the applicability of the control scheme in LCGT for the operation mode, the deterioration of the quantum noise limited sensitivity is calculated here. The degree to which various feedback signals contribute to the deterioration of a detector sensitivity is estimated in detail [10]. Here the largest two contribution factors are considered. The procedure is as follows. First, the signal matrix for LCGT is calculated to show the two largest contribution factors. Secondly the shot noise level of the DOFs that plays a role here is calculated. And finally the deterioration ratio is calculated.

A. Theoretical signal matrix for LCGT

Table III shows a theoretical DC signal matrix obtained by applying the control scheme to LCGT. The values are normalized by the amplitude of the signal that should be obtained by the detection system shown in each raw. The values of the signals are shown in the column 6 for later use.

The LCGT parameters used here are listed in Table IV. r_x represents the amplitude reflectivity of a mirror x, m_y represents the modulation depth of the y sideband. These values are used to estimate the shot noise level throughout the discussion. Note that the pick off mirror is the one that is used to obtain l_s DOF signal. For this calculation maximum power on a PD is limited to be 100mW, and at DP 6% of the power is used for the l_- signal detection purpose.

The largest contribution comes from the path $C_{24} \to C_{22}$, where C_{ij} represents the matrix element of the i-th raw and j-th column. When the control signal of the l_- DOF fluctuates due to the shot noise that appears in the photo-detection process at DP(DD), the noise induces the l_- DOF motion via its feedback loop. The portion of the motion which is represented by the element C_{24}, appears in the control signal of the L_- DOF, consequently adding the shot noise on the control signal of the l_- to that of the L_- DOF. This is the direct path. Other possible direct paths, such as those from the elements C_{23} and C_{25} is very small as the matrix elements are very close to zero, and so are neglected throughout the following discussion.

Second largest factors are via the paths $C_{43} \to C_{44}$ and $C_{45} \to C_{44}$, which will then follow the direct path $C_{24} \to C_{22}$. In the same manner as in the direct path, the l_+ and l_s DOFs fluctuate due to the shot noise that is present in their detection processes, and induce the corresponding motions. The portion of them represented by the elements C_{43} and C_{45} will appear in the control signal of the l_- DOF, which will then induce the l_- DOF motion via its feedback loop, which will follow the direct path.

B. Shot noise level at various ports

The signal to noise ratio (SNR) of the quantum noise for L_- DOF of a zero-detuning RSE interferometer is calculated using formulas given in [11]. The quantum noise is given by the sum of the radiation pressure noise and the snot noise in the formula, and the two can be calculated separately for our purpose to consider only the shot noise part for now. Note that we assume a homodyne detection whereas the designed control scheme for LCGT uses heterodyne detection scheme. The discrepancy between the two model is found to be negligible for this discussion. Here, the ratio between the SNR of the shot noise for l_-, l_+, and l_s and that for L_- DOF are given as follows.

$$\text{(SNR for } l_-) : (\text{SNR for } L_-) = \left| \frac{S_2}{N_{DP}} \right| : \left| \frac{S_4}{N_{dp}} \right| \quad (1)$$

$$\text{(SNR for } l_+) : (\text{SNR for } L_-) = \left| \frac{S_2}{N_{DP}} \right| : \left| \frac{S_3}{N_{bp}} \right| \quad (2)$$

$$\text{(SNR for } l_s) : (\text{SNR for } L_-) = \left| \frac{S_2}{N_{DP}} \right| : \left| \frac{S_5}{N_{po}} \right| \quad (3)$$

where S_i represents the DC signal value which are shown in i-th raw in the column 6. In general S_2 has a frequency response which is flat up to a cut-off frequency of the FP arm cavity, and it rolls off as the inverse of the frequency. N_{DP}, N_{dp}, N_{bp}, and N_{po} represent the shot noise at DP(SD), DP(DD), BP(DD), and PO(DD), respectively. Finally the amount that will contribute to the sensitivity is estimated as follows.

$$\text{(Contribution } l_-) = (\text{SNR for } l_-) \times C_{24} K_{l_-} \quad (4)$$

$$\text{(Contribution } l_+) = (\text{SNR for } l_+) \times C_{43} K_{l_+} C_{24} K_{l_-} \quad (5)$$

$$\text{(Contribution } l_s) = (\text{SNR for } l_s) \times C_{45} K_{l_s} C_{24} K_{l_-} \quad (6)$$

where $K_{l_-} = G_{l_-}/1 + G_{l_-}$, etc. are closed loop gains of the corresponding DOF feedback system where G_{1_-}

TABLE III: LCGT normalized sinal matrix

	L_+	L_-	l_+	l_-	l_s	signal[W/m]
BP(SD)	1	2.5×10^{-8}	-3.4×10^{-3}	2.4×10^{-5}	2.4×10^{-3}	-9.5×10^7
DP(SD)	0^a	1	0^a	1.0×10^{-3}	0^a	6.7×10^{10}
BP(DD)	-1.8×10^{-3}	-6.5×10^{-7}	1	-6.3×10^{-4}	-0.73	3.4×10^4
DP(DD)	0^a	1.2×10^{-3}	-1.5×10^{-8}	1	1.4×10^{-8}	3.1×10^5
PO(DD)	-4.8×10^{-4}	1.1×10^{-7}	1.0	1.1×10^{-4}	1	2.3×10^4

$^a 0 :< \sim 10^{-11}$

TABLE IV: LCGT parameters

|	
Power at BS	780W
r_{ITM}	$\sqrt{0.996}$
r_{ETM}	$\sqrt{0.99995}$
r_{PRM}	$\sqrt{0.8}$
r_{SEM}	$\sqrt{0.77}$
$r_{\mathrm{pick\ off}}$	$\sqrt{1.35} \times 10^{-2}$
loss in ITMs and ETMs	20ppm
Modulation frequency(PM)	10MHz
Modulation frequency(AM)	60MHz
m_{PM}	0.2
m_{AM}	0.2

etc. are open loop gains of the system, which are assumed to have $f^{-1.5}$ frequency dependance around and above the unity gain frequency at 10Hz for this estimation. The very low unity gain frequency estimation comes from the fact that the LCGT cite has very low seismic noise level and the Seismic Attenuation System (SAS) will be installed to strongly decouple the test masses and the seismic motion.

As a result of the estimation, the shot noise contribution from the l_+ and the l_s are found to be negligible. This comes from the fact that the matrix elements C_{43} and C_{45} are small enough. The contribution from the l_- is found not to deteriorate the quantum noise limited sensitivity as shown in Fig. 10. The shot noise carried by the feedback signal of l_- can be reduced in order to further safely run the detector at its design sensitivity, by using a feed-forward technique with which the shot noise on l_- DOF is linearly subtracted from that on the L_- DOF. The technique has been demonstrated in detectors such as LIGO, Virgo and TAMA300 where a reduction of $\sim 1/30$ has been successfully achieved.

VI. CONCLUSION

A new control scheme has been developed for LCGT, and a PRZD RSE interferometer has been successfully controlled with the scheme. This result has shown that the LCGT can use a PRZD RSE interferometer as its optical configuration and use our control scheme to lock the interferometer. The control scheme is also shown not to deteriorate the quantum noise limited sensitivity.
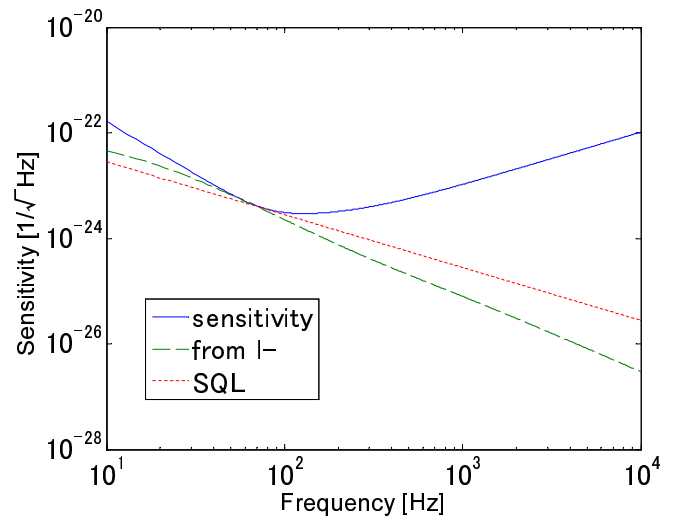
FIG. 10: Contribution of shot noise on l_-

This is one of the important steps towards the successful operation of the LCGT detector.

[1] D. Sigg (LIGO Science Collaboration), Class. Quantum. Grav. **23**, S51 (2006).

[2] H. Lück, M. Hewitson, P. Ajith, B. Allen, P. Aufmuth, C. Aulbert, S. Babak, R. Balasubramanian, B. W Barr. S. Berukoff *et al.*, Class. Quantum. Grav. **23**, S71 (2006).

[3] F. Acernese, P. Amico, M. Al-Shourbagy, S. Aoudia, S. Avino1, D. Babusci, G. Ballardin, F. Barone, L. Barsotti, M. Barsuglia *et al.*, Class. Quantum. Grav. **23**, S63 (2006).

[4] M. Ando and the TAMA Collaboration, Class. Quantum. Grav. **22**, S881 (2005).

[5] P. Fritschel, Proc. SPIE Int. Soc. Opt. Eng. **4856**, p.282 (2002).

[6] K. Kuroda, M. Ohashi, S. Miyoki, D. Tatsumi, S. Sato, H. Ishizuka, M.-K. Fujimoto, S. Kawamura, R. Takahashi, T. Yamazaki *et al*, Int. J. Mod. Phys. **D 8**, 557 (1999).

[7] S. Sato, S. Kawamura, K. Kokeyama, F. Kawazoe, and K. Somiya, Phys. Rev. D **75**, 082004 (2007).

[8] F. Kawazoe, K. Kokeyama, S. Sato, O. Miyakawa, K. Somiya, M. Fukushima, N. Arai, S. Kawamura and A. Sugamoto, J. Phys.: Conf. Series **32**, 380 (2006).

[9] C. M. Caves, Phys. Rev. D **23**, 231693 (1981).

[10] K. Somiya, O. Miyakawa, P. Fritschel, and R. Adhikali, Length Sensing and Control for AdLIGO.T060272.00.I0 (2006).

[11] A. Buonanno and Y. Chen, Phys. Rev. D **64**, 042006 (2001).

[12] One thing to note is that the amplitude of the L_+ signal which mixes at PO(DD) system is comparable to the main signal l_s. It is found out by simulation that this is because the macroscopic length of the arm cavity are such that the AM sidebands are not very much away from the resonance peaks of the cavity. When choosing the length the size of the existing camber limited the freedom of choosing the best possible design, and so the optimum design is a compromising one. Therefore the size of the unwanted signal can be reduced by choosing the right length of the FP arm cavity, thus it will not be a problem in a real detector such as LCGT.

[13] The direct lock of the FP arm cavities' two DOFs, the common, L_+, and the differential, L_-, has been realized without one additional step (locking the individual arms with each control signal then switch the control servos for those of the common and the differential control). This is because often one of the two FP arm cavities is locked with the control signal for the L_+ DOF first, and as soon as the other FP arm cavity's DOF is close to its operating point the L_- DOF is controlled, consequently switching the L_+ control signal to lock the L_+ DOF. Typically the time interval between the lock of one FP arm cavity and both cavities is less than a second.